

Deep learning for evaluating the effects of a layout of photon sensors on event reconstructions

Chang-Wei Loh,^a Zhi-Qiang Qian,^{a,2} You-Hang Liu,^a De-Wen Cao,^a Rui Zhang,^a Wei Wang,^a Hai-Bo Yang^a and Ming Qi^{a,1}

^a*Nanjing University, 22 Hankou Road, Nanjing, Jiangsu, China*

E-mail: qming@nju.edu.cn

ABSTRACT: We provide a fast approach incorporating the usage of deep learning for evaluating the effects of a layout of photon sensors in an antineutrino detector on the event reconstruction performance therein, which in turn could help to optimize the potential of an experiment. Applying this to the Daya Bay detector, we found that the photomultiplier tubes (PMTs) have different relative importance to the vertex reconstruction. We found that the vertex position resolutions follow approximately a multi-exponential relationship with respect to the number of PMTs and hence, the coverage.

¹Corresponding author

²Coauthor

Contents

1	Introduction	1
2	Recursive Search	2
3	Deep Neural Network	3
4	Results	5
5	Conclusions and future work	8

1 Introduction

Optimization of photon sensors such as photomultiplier tubes (PMTs), be it their expected sizes, locations and the total number of sensors in antineutrino detectors, including Daya Bay [1], Double Chooz [2], RENO [3] and JUNO [4] are of interest as these sensors are the information gatherers through which we can identify antineutrino interaction events. Building on the optimization theme, we could ask the following: suppose we have N number of locations for the installation of k number of PMTs ($k \leq N$), how can we identify the optimal locations for these PMTs such that the event interaction vertex reconstruction is optimal given only these k PMTs in the detector? Upon solving this, we could then use this knowledge to optimize the designing of antineutrino detectors or planning of existing detector upgrade programs, understanding the impact of each sensor on the interaction vertex reconstruction, and in improving any signal-background vertex-based discrimination criteria. The knowledge on event vertex positions also plays a role in correcting the position-dependent energy response in the detector, which is imperative to neutrino oscillation precision measurements. Beyond high-energy physics, optimization of sensor placements has been studied in areas ranging from water network distributions [5] to fault detections [6]. In this work, a model of the Daya Bay detector is chosen as a test case to understand the impact of a layout of PMTs to event position vertex reconstructions in a detector.

The Daya Bay antineutrino detectors are liquid scintillator detectors with a physics program focusing on the precision measurement of the neutrino mixing angle θ_{13} with reactor antineutrinos. Each Daya Bay detector consists of three concentric cylindrical tanks: an inner acrylic vessel (IAV) containing gadolinium (Gd)-doped liquid scintillator, an outer acrylic vessel (OAV) containing undoped liquid scintillator which surrounds the IAV, and a stainless steel vessel (SSV) which surrounds the IAV and OAV. With this design, the detectors could detect the interaction of the antineutrinos and the scintillator via inverse beta decay (IBD) reactions:

$$\bar{\nu}_e + p \rightarrow e^+ + n. \quad (1.1)$$

The emitted positron then undergoes ionization processes in the liquid scintillator before annihilating with an electron producing a prompt signal with an energy deposition in the range of 1 - 8 MeV.

The deposited energy is converted to scintillation photons which are then collected by the PMTs. As the positron displacement prior to the annihilation is negligible, the interaction vertex of the prompt signal can be assumed to be the antineutrino IBD interaction vertex. However, the neutron thermalizes and diffuses before being captured on either a proton or Gd with a mean capture time of $\sim 30 \mu s$ in the Gd-doped liquid scintillator and $\sim 200 \mu s$ in the undoped liquid scintillator, giving rise to a delayed signal. A total of 192 Hamamatsu R5912 8-inch PMTs [7], arranged in a layout with 8 rows and 24 columns, are installed on the vertical wall of the SSV pointing inward towards the OAV and IAV forming a total of 6% photodetector coverage. Located above and below the OAV are reflective panels that serve to redirect scintillation light towards the PMTs thereby increasing the photon collection efficiency to 12% effectively.

In order to study the effects of PMT layouts to an event reconstruction and hence the optimization thereof, we opt to use deep learning [8] to perform the IBD interaction vertex reconstruction. Deep learning is a class of machine learning, which is especially adept at leveraging large datasets to compute human-comprehensible quantities by learning the various degrees of correlations within. Notably, it can, on its own, learn to discover functional relationships from the data without *a priori* given, effectively forming a mapping from the inputs to a quantity of interest. In other words, deep learning seeks to model the quantity of interest y using a vector of inputs x with $DL(x, p) = y$, where p are parameters of the deep network; their numerical values found by minimizing the error between the predicted y' and y . Deep learning machine architectures, commonly known as deep neural networks (DNN), are based on artificial neural networks [9] but deeper in terms of the number of hidden layers, and are more flexible in terms of how each neuron is connected to other neurons.

The ubiquity of deep learning and its significant success over traditional methods across disparate fields [10–12] in discovering patterns is surprising. However, this may well be due, in part, to that our universe operates on simple physical properties [13]. In high-energy physics, deep learning has demonstrated its prospective use in jets [14, 15], as part of the signal-background discrimination toolkit in the search for beyond the Standard Model particles [16] and Higgs bosons [17], and in the Daya Bay neutrino experiment [18–22].

2 Recursive Search

As mentioned in Section 1, we wish to search for the k most important locations corresponding to k PMTs installed therein from the N total possible locations in the detector in determining the vertex position V of events collected from the detector. N is a free parameter which could be chosen during the detector design and simulation stage. Denoting the set containing the k number of optimal locations as the optimal set S_k^* , this implies that we should find the set S_k^* such that the vertex reconstruction error is minimized. However, finding such k locations simultaneously is a task confounded by a computation that grows exponentially with k . Alternatively, we could search for an approximation to S_k^* by recursively finding the optimal PMT location one at a time, which can be achieved using deep learning. Since searching for the optimal location is equivalent to searching for the optimal PMT at that particular location, the phrase "kth optimal PMT" will be used in this work as a shorthand for "kth optimal PMT location".

Let the true position of the IBD prompt events be $V_{true} = \{x_{true}, y_{true}, z_{true}\}$; the predicted position using DNN as $V_{pred} = \{x_{pred}, y_{pred}, z_{pred}\}$, then in a recursive search, the k -th optimal

PMT, PMT_k^* will be the one that maximizes the improvement in the resolution σ of the residual distribution conditioned on already known the $(k - 1)$ other PMTs found through the recursive search, i.e., $\{PMT_{k-1}^*, PMT_{k-2}^*, \dots, PMT_1^*\}$, and where the residual is $V_{pred} - V_{true}$. Namely,

$$PMT_k^* = \underset{P_k \in N \setminus S_{k-1}^{recu}}{\operatorname{argmin}} \sigma(PMT_k, S_{k-1}^{recu}), \quad (2.1)$$

where $S_{k-1}^{recu} = \{PMT_{k-1}^*, \dots, PMT_1^*\}$ and N is the set containing all the PMTs. Using Equation 2.1, PMTs could be progressively added into a larger and larger subset S defining the best set found by the algorithm. Alternatively, one could perform a backward elimination: starting from the set with all PMTs, and progressively eliminating the most "unimportant" PMT. At the conclusion of this recursive search, we obtain a curve of the event reconstruction resolution vs. the number of PMTs used for the reconstruction thereof.

3 Deep Neural Network

In our approach utilizing DNNs, we used a Monte Carlo dataset comprising 2 million IBD prompt events obtained from a Daya Bay detector model which were randomly partitioned into a training set, a validation set and a test set with a split ratio of 6:1:3. The validation set is used for the early stopping of the DNN training to prevent overfitting or underfitting of the data [23]. The parameter N as defined in Section 2 would be 192 corresponding to the 192 PMT locations in the Daya Bay detector model. The charge information of the 192 PMTs are fed into the DNN as its inputs, and the output is the predicted vertex location V_{pred} . To train the DNN, we used the mean square error (MSE) loss function to measure the error between the predicted and the truth vertex positions:

$$MSE = \frac{1}{T} \sum_{j=1}^T (v_{ij_{pred}} - v_{ij_{true}})^2, \quad (3.1)$$

where T is the number of events, $v_{ij_{pred}}$ and $v_{ij_{true}}$ are the predicted and truth values for the i -th coordinate of the j -th event vertex respectively ($i = x, y, z$). The MSE was minimized to obtain the optimal DNN parameters. The minimization is typically done with a gradient descent method [24] involving the gradient of the loss function with respect to the DNN parameters, including the weights of each neuron.

A representative image of the 8×24 charge pattern due to an electron-positron annihilation event in the Daya Bay detector is shown in Figure 1. The color of each rectangle corresponds to the charge collected by the PMT at the corresponding ring and column location.

The efficacy of deep learning to predict the position of the IBD prompt events can be demonstrated by the residual distributions shown in Figure 2 where the charge information of the 192 PMTs are fed into a DNN as its inputs. The DNN used here to obtain V_{pred} consists of multiple fully-connected layers with ReLU [25] hidden neurons. The resolutions as obtained from the Gaussian fit to the residual distributions are 67 mm and 80 mm for $(x_{pred} - x_{true})$ and $(z_{pred} - z_{true})$ respectively.

A straightforward and brute force use of Equation 2.1 in a recursive search using a DNN to identify PMT_k^* would be to check over all the remaining PMTs not in the optimal set S_{k-1}^* and separately construct the residual distributions; picking the one giving the best resolution for a

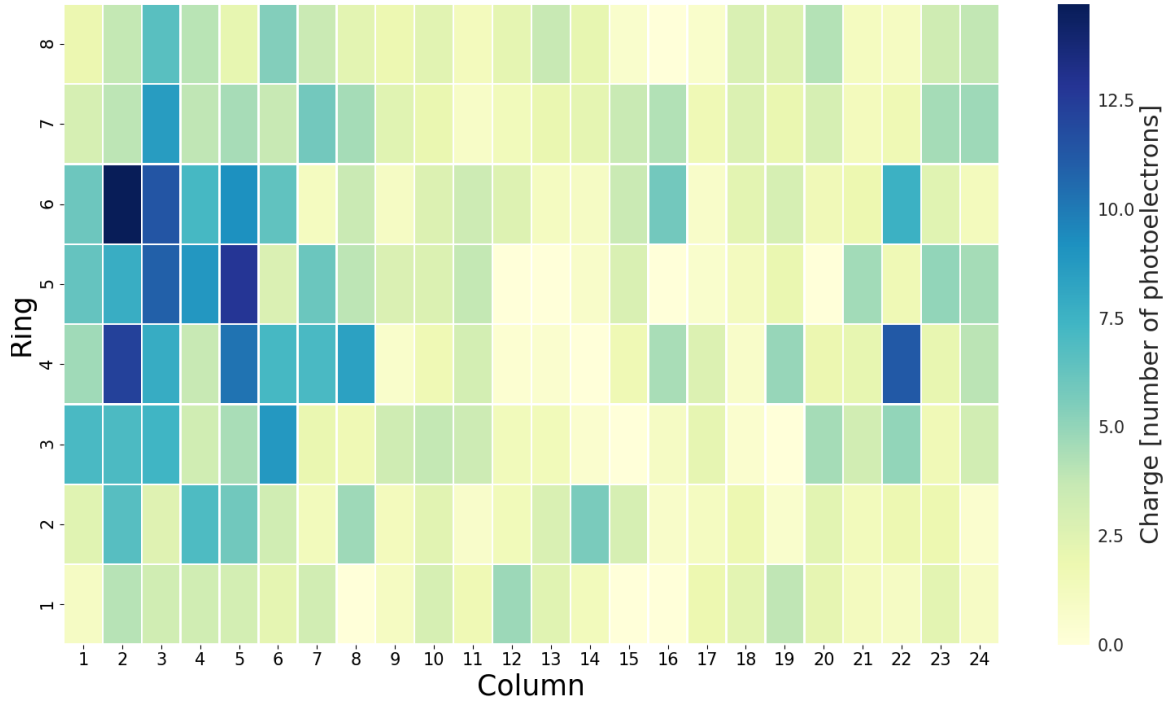


Figure 1. Charge distribution of a simulated event in the Daya Bay detector as collected by the 192 PMTs. The color scale shows the charge magnitudes. Charge information like these are fed into the DNN as inputs.

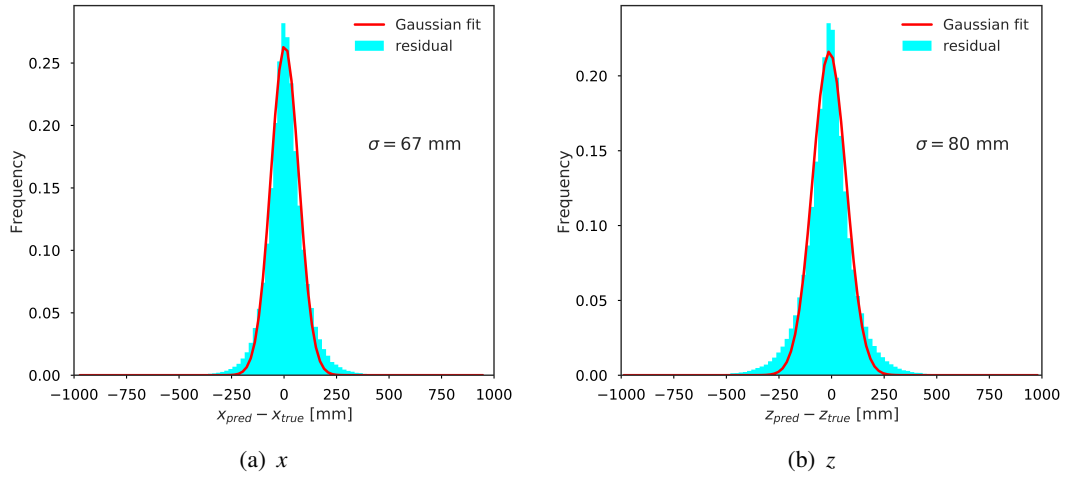


Figure 2. Residual distributions for x and z using all 192 PMT charge information.

particular coordinate in V_{true} . For this brute force search, we used a DNN architecture similar to the aforementioned DNN. The input layer will contain neurons with charge information from the

already-chosen PMTs, i.e., those in S_{k-1}^{recu} , plus a candidate PMT, i.e., PMT_k . The computation time for such a search grows quadratically with the total number of PMTs in the detector. Such a brute force search is clearly not scalable. Hence, in this work, we have also used a fast approach to approximate the brute force search but which mitigates the non-scalability of the latter.

This fast approach integrates a DNN component from the autoencoder architecture [26]: a bottleneck layer with a single neuron, as shown in Figure 3. In this bottleneck DNN architecture, the remaining candidate PMTs not in S_{k-1}^{recu} are forced to connect to the bottleneck neuron before being given to the fully-connected layers as inputs, effectively demanding the DNN to search for the best weights associated with each of these PMTs. The weights are constrained to be positive values. The PMT with the largest weight indicates that the reconstruction of the position of the IBD prompt events relies the heaviest on this PMT compared to the rest of the candidate PMTs. Hence, this PMT would be our optimal k -th PMT, PMT_k^* . Crucially, this DNN only needs to be trained once to identify PMT_k^* no matter the value of k , whereas the brute force DNN needs to be trained $(N - k)$ times, once for each remaining candidate PMT.

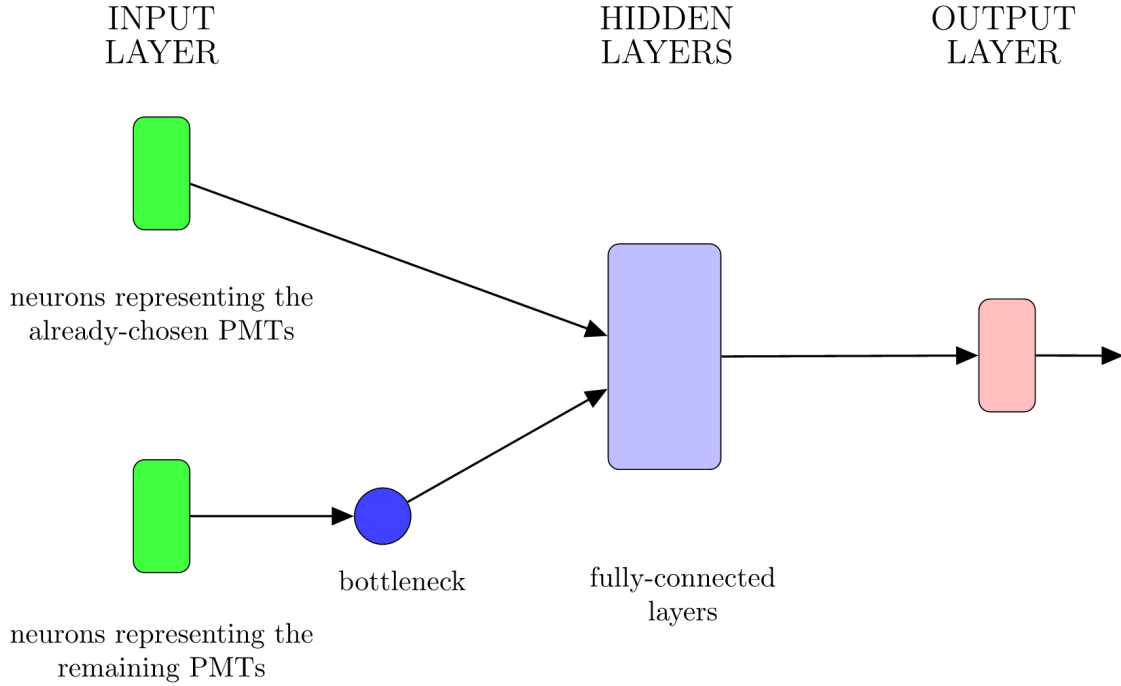


Figure 3. DNN architecture consisting of a bottleneck neuron.

4 Results

The heatmap in Figures 4 show the resolutions as obtained from the residual distributions corresponding to using only one PMT for training and determining the vertex location of the antineutrino IBD interaction using the brute force search. Specifically, the resolution pertaining to using each PMT is indicated by a value from the color scale. Clearly, some PMTs receive more information about the vertex position than others. The first most important PMT from the brute force search, i.e.

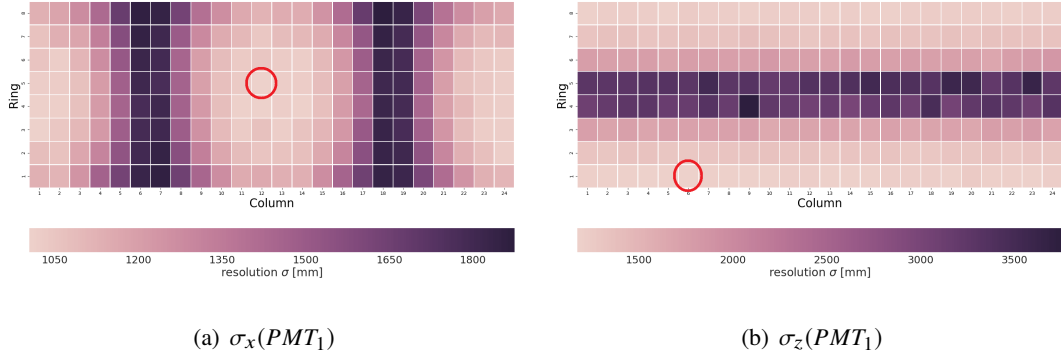


Figure 4. Resolution σ corresponding to using each individual PMT for (a) x and (b) z , using the brute force search. In each heatmap, the circled PMT corresponds to the best resolution amongst all the 192 PMTs.

PMT_1^{brute*} , is chosen as the one having the smallest color value in the heatmap. The variation in resolution for the x -direction by column is due to the use of σ_x rather than σ_r . The reconstruction shows that the optimal PMT is different for the x -direction and the z -direction. If needed, one could average the resolutions in the x and z directions to obtain the average optimal PMT. The heatmap pattern for the y -direction is similar to the x -direction, but with the dark region in the x -direction being the light region in the y -direction and vice versa, reflecting that the x and y depend on $\cos \phi$ and $\sin \phi$ respectively in a cylindrical coordinate system, i.e. a $\pi/2$ shift in difference between x and y . In Figure 5, the heatmap shows the weight corresponding to each PMT as obtained from the bottleneck neuron when searching for the first most important PMT.

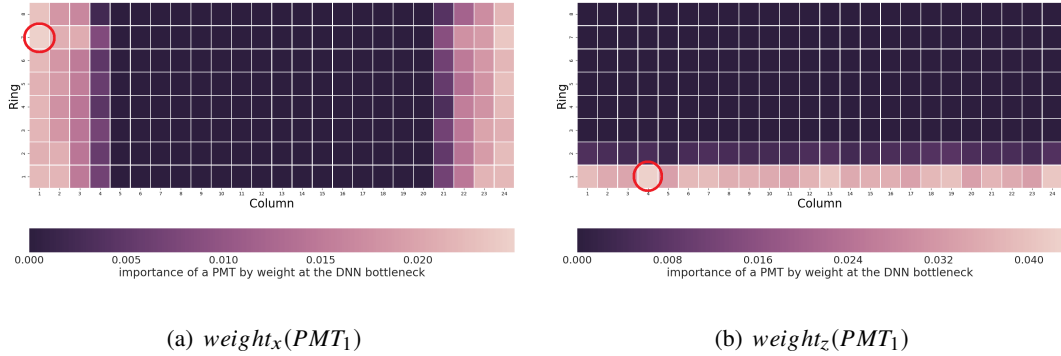


Figure 5. Weights as given by the bottleneck neuron corresponding to each PMT for (a) x and (b) z using the bottleneck DNN. In each heatmap, the circled PMT corresponds to the largest weight in the heatmap amongst all the 192 PMTs, indicating that it is the most heavily used PMT in the DNN during the vertex reconstruction.

A higher weight indicates that the PMT has a larger impact on the vertex reconstruction. The PMT with the largest weight is identified as the most important PMT, PMT_1^{bneck*} . Ideally, we would like to constrain the weights to be discrete at the bottleneck, i.e., to be either 0 or 1, where weight is 1 for the most important PMT and 0 for the rest even during the training of the DNN. However, such

a constraint is non-differentiable and non-continuous with respect to the loss function which would render DNN parameter optimization using gradient descent algorithms unfeasible. Comparing Figure 4 and 5, the brute force and the bottleneck DNN have chosen different PMTs as their optimal PMTs possibly due to degeneracies in the detector. For example, in the z -direction, the PMTs at the top and bottom rings should produce the same resolution. Our suspect is that during the training of the bottleneck DNN, some information sharing between a subset of PMTs, in which the DNN thinks their information values are similar, are unavoidable. Hence, the bottleneck neuron contains information from not one but a subset of PMTs, i.e. the importance by weights of each PMT could be partially "shared" amongst several PMTs. Further understanding of these are being conducted. Figures 6 and 7 are the results as obtained from the brute force and bottleneck DNN approach respectively while searching for the second most important PMT after having found the first most important PMT.

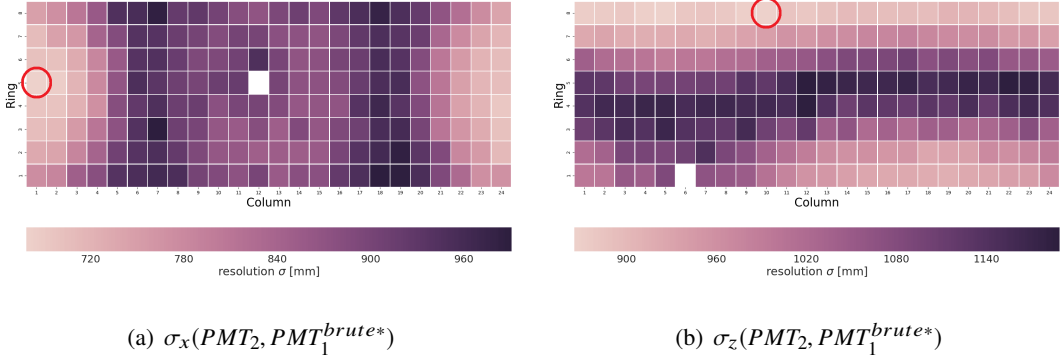


Figure 6. Resolution σ corresponding to using the charge information from the most important PMT as identified previously and a second candidate PMT for (a) x and (b) z . The first PMT as found by the previous round, PMT_1^{brute*} using the brute force search is whitened in each Figure. In each of the heatmap, the circled PMT, PMT_2^* corresponds to the best resolution when considering the said PMT and the first optimal PMT found previously for the vertex reconstruction.

Figure 8 shows the residual curve for x and z as a function of the number of PMTs used in the reconstruction. Using an Nvidia Tesla P40 GPU, we estimated that it would take about 60 days to complete the entire residual curve with the brute force search, whereas it took about one day to complete with the bottleneck DNN. Resolutions from random choice of PMTs are also included in the Figures as a comparison to the result from the bottleneck DNN. An empirical fit to the bottleneck DNN results is done with a triple exponential fit. It can be clearly seen that there is a diminishing return on the improvement in the vertex resolution when adding additional PMTs to an existing set of PMTs, which is an implication of the submodular [27] nature of the Gaussian standard deviation and its relationship to the information entropy, $H = \log \sigma + 0.5 \log(2\pi e)$. Succinctly, the submodularity of the Gaussian standard deviation, i.e. the resolution in this case shows that there is less new information that could be gained from adding a new PMT to a larger set of already-chosen PMTs than to a smaller set. As all the PMTs in the Daya Bay detector are of the same size and model, Figure 8 could also be interpreted as the residual curve being a function of the detector coverage.

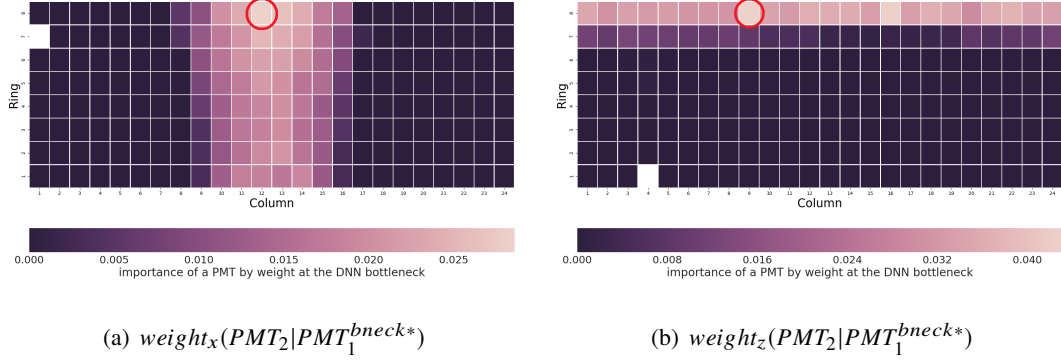


Figure 7. Weights as given by the bottleneck neuron corresponding to using a second candidate PMT, and the most important PMT, PMT_1^{bneck*} as identified previously for (a) x and (b) z . PMT_1^{bneck*} is whitened in each Figure. In each of the heatmap, the circled PMT, PMT_2^* corresponds to the largest weight amongst the remaining 191 PMTs given that the first optimal PMT has been identified with the bottleneck DNN.

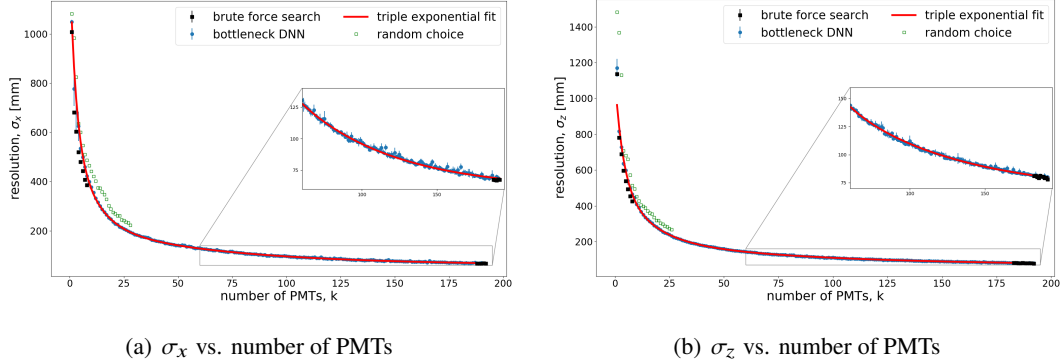


Figure 8. Residual curves for x (left Figure) and z (right Figure) as a function of the number of PMTs used in the reconstruction. The results plotted as solid squares are those from the brute force search. An empirical fit to the bottleneck DNN results was done with a triple exponential. Resolutions from random choice of PMTs are shown as empty squares. A zoom-in on the residual curves is also shown in the Figures.

5 Conclusions and future work

In this work, we provide a fast approach using a deep neural network with a bottleneck neuron to uncover the layout effects of photon sensors such as PMTs on the vertex resolutions in an antineutrino detector. The results have been compared with a brute force search. Our inputs are the simulated charge information of the Daya Bay PMTs. We found that the vertex resolution of the event reconstruction is approximately a multi-exponentially decreasing function with respect to the number of PMTs and hence also, the coverage. In future work, we envisage the possibility of incorporating the temporal information, i.e., the time of arrival of each photon in addition to the charge information to reconstruct the vertices. In addition, one could also study the size of the PMT needed alongside its installation location corresponding to the optimal event vertex reconstruction resolution. It would be of interest to study the effect of a set of PMTs based on the event energy in

lieu of the vertex. Although studying the energy would need modifications to the deep network, the energy resolution is generally more important than the vertex resolution when considering physics sensitivity, and thereby impacting the design of future antineutrino detectors including JUNO.

Acknowledgments

We thank Shen-Jian Chen for providing the computing facilities, including an Nvidia Tesla P40 GPU to complete this work. We would also like to thank Chao Zhang, Zhe Wang, Samuel Kohn, the Daya Bay ACC and the entire Collaboration for their time and comments. This work was supported by the National 973 Project Foundation of the Ministry of Science and Technology of China (Contract No. 2013CB834300).

References

- [1] J. Cao, K.-B. Luk, "An overview of the Daya Bay reactor neutrino experiment", Nuclear Physics B 908 (2016) 62 – 73. Neutrino Oscillations: Celebrating the Nobel Prize in Physics 2015.
- [2] Double Chooz collaboration. Y. Abe, et al., *Improved measurements of the neutrino mixing angle θ_{13} with the Double Chooz detector*, JHEP 2014 (2014) 86.
- [3] RENO collaboration. J. Choi, et al., *Observation of Energy and Baseline Dependent Reactor Antineutrino Disappearance in the RENO Experiment*, Phys. Rev. Lett. 116 (2016) 211801.
- [4] JUNO collaboration. F. An, et al., *Neutrino physics with JUNO*, Journal of Physics G: Nuclear and Particle Physics 43 (2016) 030401.
- [5] A. Krause, et al., *Efficient Sensor Placement Optimization for Securing Large Water Distribution Networks*, Journal of Water Resources Planning and Management 134 (2008) 516–526.
- [6] K. Worden, A. P. Burrows, *Optimal Sensor Placement for Fault Detection*, Engineering Structures 23 (2000) 885–901.
- [7] J. Soren, et al., *PMT waveform modeling at the Daya Bay experiment*, Chinese Physics C 36 (2012) 733.
- [8] Y. Lecun, Y. Bengio, G. Hinton, *Deep Learning*, Nature 521 (2015) 436–444.
- [9] W. S. McCulloch, W. Pitts, *A Logical Calculus of the Ideas Immanent in Nervous Activity*, The Bulletin of Math. Biophys. 5 (1943) 115–133.
- [10] A. Krizhevsky, I. Sutskever, G. E. Hinton, *Imagenet Classification with Deep Convolutional Neural Networks*, in: F. Pereira, C. J. C. Burges, L. Bottou, K. Q. Weinberger (Eds.), Advances in Neural Information Processing Systems 25, 2012, pp. 1097–1105.
- [11] D. Silver, et al., *Mastering the Game of Go with Deep Neural Networks and Tree Search*, Nature 529 (2016) 484–489.
- [12] F. Buggenthin, et al., *Prospective Identification of Hematopoietic Lineage Choice by Deep Learning*, Nature Methods 14 (2017) 403–406.
- [13] H. W. Lin, M. Tegmark, D. Rolnick, *Why Does Deep and Cheap Learning Work So Well?*, arXiv (1608.08225).
- [14] D. Guest, et al., *Jet Flavor Classification in High-Energy Physics with Deep Neural Networks*, Phys. Rev. D94 (2016) 112002.

- [15] P. T. Komiske, E. M. Metodiev, M. D. Schwartz, *Deep Learning in Color: Towards Automated Quark/Gluon Jet Discrimination*, JHEP 01 (2017).
- [16] P. Baldi, P. Sadowski, D. Whiteson, *Searching for Exotic Particles in High-Energy Physics with Deep Learning*, Nature Comm. 5 (2014).
- [17] P. Baldi, P. Sadowski, D. Whiteson, *Enhanced Higgs Boson to Tau+ Tau- Search with Deep Learning*, Phys. Rev. Lett. 114 (2015).
- [18] S. Kohn, *Understanding Backgrounds using Deep Learning at the Daya Bay Experiment*, 2017. Work presented at the 28th International Symposium on Lepton Photon Interactions at High Energies.
- [19] MiniBoone collaboration. R. Acciarri, et al., *Convolutional neural networks applied to neutrino events in a liquid argon time projection chamber*, JINST 12 (2017) P03011.
- [20] A. Aurisano, et al., *A convolutional neural network neutrino event classifier*, JINST 11 (2016) P09001.
- [21] NEXT collaboration. J. Renner, et al., *Background rejection in NEXT using deep neural networks*, Journal of Instrumentation 12 (2017) T01004.
- [22] E. Racah, et al., *Revealing Fundamental Physics from the Daya Bay Neutrino Experiment using Deep Neural Networks*, in: *2016 15th IEEE International Conference on Machine Learning and Applications (ICMLA)*, pp. 892–897.
- [23] L. Prechelt, *Early stopping-but when?*, in: *Neural Networks: Tricks of the Trade*, Springer, 1998, pp. 56–69.
- [24] D. E. Rumelhart, et al., *Learning representations by back-propagating errors*, Nature 323 (1986) 533–536.
- [25] V. Nair, G. Hinton, *Rectified Linear Units Improve Restricted Boltzmann Machines*, in: J. Furnkranz, T. Joachims (Eds.), *Proceedings of the 27th International Conference on Machine Learning (ICML-10)*, Omnipress, 2010, pp. 807–814.
- [26] G. E. Hinton, R. S. Zemel, *Autoencoders, Minimum Description Length and Helmholtz Free Energy*, in: J. D. Cowan, G. Tesauro, J. Alspector (Eds.), *Advances in Neural Information Processing Systems 6*, Morgan-Kaufmann, 1994, pp. 3–10.
- [27] G. L. Nemhauser, et al., *An analysis of approximations for maximizing submodular set functions-I*, Mathematical Programming 14 (1978) 265–294.